Available online at www.sciencedirect.com
SCIENCE DIRECT
Journal of Magnetic Resonance 178 (2006) 136–141
JMR Journal of Magnetic Resonance
www.elsevier.com/locate/jmr

Spatially resolved measurement of rock core porosity

F. Marica [a], Q. Chen [a], A. Hamilton [b], C. Hall [b], T. Al [c], B.J. Balcom [a,*]

[a] MRI Centre, Department of Physics, University of New Brunswick, Fredericton, NB, Canada E3B 5A3
[b] Centre for Materials Science and Engineering, The University of Edinburgh, Edinburgh, Scotland, UK
[c] Department of Geology, University of New Brunswick, Fredericton, NB, Canada E3B 5A3

Received 11 April 2005; revised 9 September 2005
Available online 7 October 2005

Abstract

Density weighted, centric scan, Conical SPRITE MRI techniques are applied in the current work for local porosity measurements in fluid saturated porous media. The methodology is tested on a series of sandstone core samples. These samples vary in both porosity and degree of local heterogeneity due to bedding plane structure. The MRI porosity measurement is in good agreement with traditional gravimetric measurements of porosity. Spatially resolved porosity measurements reveal significant porosity variation in some samples. This novel MRI technique should have applications to the characterization of local porosity in a wide variety of porous media.

Keywords: MRI; Conical SPRITE; Water content; Porous media; Porosity

1. Introduction

1.1. Porosity

Porosity is one of the most fundamental parameters describing porous media. Porosity of sedimentary porous media is of great interest in many fields of research, e.g., in oil and natural gas extraction, in monitoring of contaminant percolation, and in characterizing the dynamics of cracking and material failure.

Porosity is defined as the ratio of the volume of pore space to the bulk volume of material and, for a saturated material, can be determined from knowledge of the quantity of fluid occupying the sample pore space [1,2]. Traditional methods for core analysis are based on bulk measurement, which will average over any heterogeneity present in the sample. In this work, we have investigated selected sandstone cores, some characterized by a significant bedding plane structure. The sandstone cores are generally heterogeneous and traditional porosity measurements on such samples are complicated by the heterogeneity.

Suitable interpretation of the magnetic resonance imaging (MRI) data can provide unprecedented opportunities for noninvasive and nondestructive measurements within porous media. Porous systems, for example, may be spatially mapped with an image contrast produced by spatial variation of magnetic resonance (MR) parameters such as the spin density and the relaxation time constants [3]. The magnitude of the ensuing MR signal, which is created by the radiofrequency (RF) pulse, is directly proportional to the amount of hydrogen present in the sample volume and provides in principle a measure of liquid-filled porosity.

1.2. Quantitative density imaging

To this point, spin–echo imaging has been the sole MRI approach to studying rock porosity [4–7]. However, there are several salient facts which adversely affect spin–echo methods applied to realistic porous media and which have limited the development and application of these methods despite the obvious opportunity. In gener-

* Corresponding author. Fax: +1 506 453 4581.
E-mail address: bjb@unb.ca (B.J. Balcom).

1090-7807/$ - see front matter © 2005 Elsevier Inc. All rights reserved.
doi:10.1016/j.jmr.2005.09.003

al, the spin–spin relaxation time T_2 is an ill conditioned parameter for MRI of realistic porous media for following reasons:

1. It is well known that the T_2 decay curves of water in porous media are not single exponential, owing to a distribution of relaxation times, related to the pore size distribution [8]. Given a realistic lower bound on the echo time of 1 ms, an estimation of the fluid density will be exceptionally difficult with T_2 lifetimes on the order of, or less than, the echo time.
2. Due to molecular self-diffusion through magnetic field gradients, most importantly the local gradients due to susceptibility inhomogeneities [9], the observed T_2 values are strongly dependent on the details of the experiment, e.g., the echo time [10,11].
3. The effect of nonuniform excitation by an RF pulse is a systematic underestimate of fluid mass by standard spin–echo MRI methods [12]. Any experiment requiring $\pi/2$ pulses, or especially π pulses, will not provide accurate signal amplitude estimates when the transverse signal lifetime is on the order of, or less then, the pulse length. For reasonable sample sizes, π pulse lengths and T_2^* signal lifetimes of the order of 100 μs in realistic porous media are quite common.

On the other hand, the effective spin–spin relaxation rate $(1/T_2^*)$ appears well behaved for realistic porous media and seems to be advantageous for FID based MRI methods. In sedimentary rocks and concretes, the experimental results [9] show that the FID decay rate $(1/T_2^*)$ is dominated by the susceptibility difference between the pore fluid and solid matrix, which results in an effective single exponential T_2^* decay. This occurs even when T_2 and T_1 (the spin–lattice relaxation time) are multi-exponential due to a distribution of pore sizes [13].

The spin–echo imaging drawbacks are avoided by FID-based imaging, taking advantage of the single exponential T_2^* and low flip-angle RF pulses. In addition, the natural measurement deadtime of a FID based MRI method, for example SPRITE [14], is reduced by more than one order of magnitude compared to spin–echo methods, which is critical, given the short transverse signal lifetimes in realistic porous media.

In this work we have performed, for the first time, detailed nondestructive MRI measurements of the local porosity in a range of sandstone cores. This MRI technique involves a pure phase encoding of the magnetization and thus allows the quantitative imaging of samples with short T_2^* (i.e., <1 ms) [15]. The centric scan SPRITE technique [16] is a fast MRI method characterized by a simplified image contrast and reduced gradient duty cycle, appropriate for overcoming the problems caused by the short T_2^* relaxation times that are associated with porous systems. The pulse sequence is illustrated in Fig. 1.

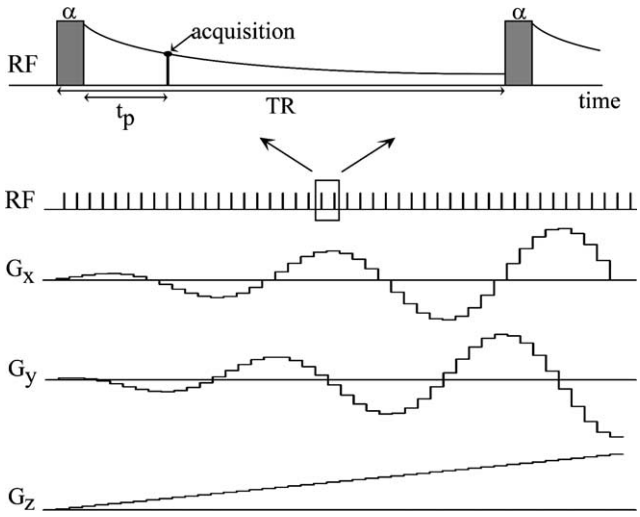

Fig. 1. Conical SPRITE MRI pulse sequence. Three phase-encoding gradients (G_x, G_y, and G_z) are employed. Oscillating X and Y gradients, as well as a ramped Z gradient, define a conical trajectory in k-space. An RF pulse is applied at each gradient level. The repetition time (TR) is the time between successive RF pulses, a single FID point is sampled at a time t_p after each RF pulse.

2. Theory

For a centric scan SPRITE experiment the local image intensity is [16]:

$$S = \rho_0 \cdot e^{-t_p/T_2^*} \cdot \sin\alpha, \quad (1)$$

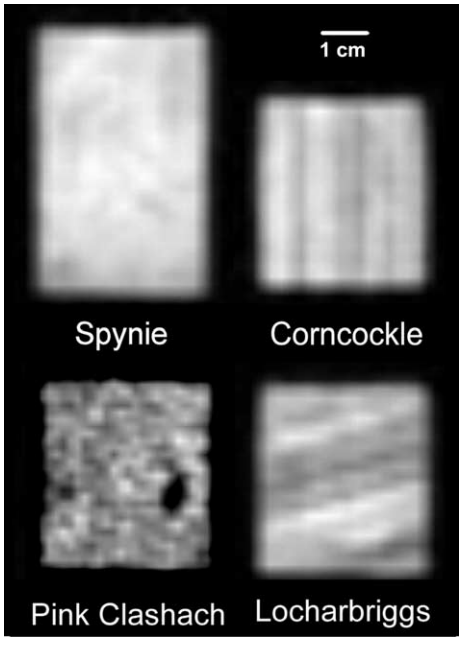

Fig. 2. 2D slices from 3D image datasets acquired at the encoding time of 100 μs for different sandstone cores, using the Conical SPRITE sequence. In these images, the bright zones represent a high MRI signal, but not necessarily a high porosity, due to T_2^* variation. The bedding plane structure in Locharbriggs, Corncockle, and Pink Clashach samples is highly heterogeneous. The images have been smoothed by zero-filling to 256^3, but are not filtered.

where ρ_0 is the spin density, t_p is the time following the radiofrequency (RF) pulse (the encoding time), T_2^* is the effective spin–spin relaxation time and α the RF pulse flip angle. The local image intensity may be calibrated by using a reference standard that is imaged with the sample.

Centric scan SPRITE can be made immune to a broad range of spin–lattice relaxation times (T_1) changes [17]. Only T_2^* and the proton density manifest themselves in the signal intensity, and they can be extracted by using a simple T_2^* mapping technique.

The single exponential T_2^* decay feature for rocks is essential to the quantitative nature of the proposed experiment. True density imaging may be achieved for samples with short T_2^* by acquiring a series of centric scan SPRITE images with variable t_p and then fitting to Eq. (1).

3. Results and discussion

The majority of fluid saturated porous sedimentary rocks, in our experience, have a single exponential T_2^* decay due to susceptibility-difference-induced field distortion. Inhomogeneous broadening thus dominates, which suggests that spin density imaging can be easily obtained by the centric scan SPRITE method [9]. 2D longitudinal slice images from 3D Conical SPRITE images for the sandstone cores studied (Locharbriggs, Spynie, Corncockle, and Pink Clashach) with water saturation of 100% are shown in Fig. 2. The Locharbriggs and Corncockle samples are fine- to medium-grained red-brown quartz sandstones, which contain minor amounts of feldspar and rare rock fragments. They are cemented by intermixed silica and hematite overgrowths. The Spynie and Clashach samples are fine grained (Spynie) and medium grained (Clashach) quartz–feldspar sandstones with minor rock fragments. They are silica cemented with the Spynie sandstone containing localized zones of iron-rich carbonate cement.

Although the observed T_2's (bulk measurements) are multi-exponential, the bulk T_2^*'s are single exponential.

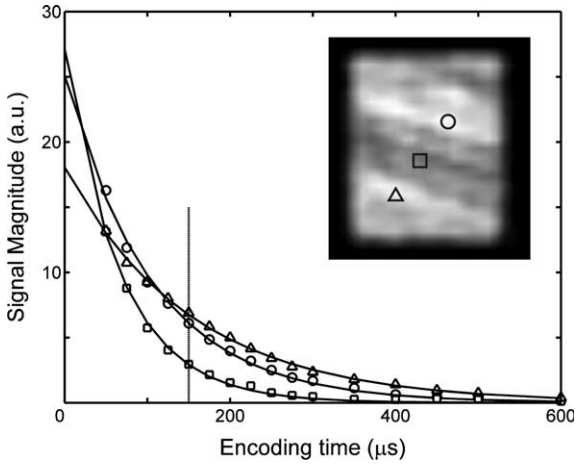

Fig. 4. The image magnitude was fit on a pixel-by-pixel basis using a monoexponential decay function. The inset was acquired at the encoding time of 150 μs (indicated by the dotted line) and the effective spin–spin relaxation times for the marked pixels are (○) $T_2^* = 106$ μs, (□) $T_2^* = 67$ μs, and (△) $T_2^* = 152$ μs. The derived porosity image was obtained from the extrapolation of the decay curves to zero encoding time.

For a water-saturated Locharbriggs sandstone the fit T_2^* was 126 μs. The bulk T_1 was 307 ms and the T_2 bulk measurement for the same sandstone gave 18 ms (62%) and 126 ms (38%) components, when fit to a biexponential decay model. For a water-saturated Spynie sandstone, the fit T_2^* was 149 μs, the bulk T_1 was 403 ms and the T_2 bulk measurement gave 10 ms (51%) and 85 ms (49%) components, when fit to a biexponential decay model. For a water-saturated Corncockle sandstone, the fit T_2^* was 125 μs, the bulk T_1 was 212 ms and the T_2 bulk measurement gave 9 ms (57%) and 67 ms (43%) components, when fit to a biexponential decay model. Finally, for a water-saturated Pink Clashach sandstone, the fit T_2^* was 321 μs, the bulk T_1 was 516 ms and the T_2 bulk measurement gave 16 ms (55%) and 72 ms (45%) components, when fit to a biexponential decay model. While in all cases we have fit

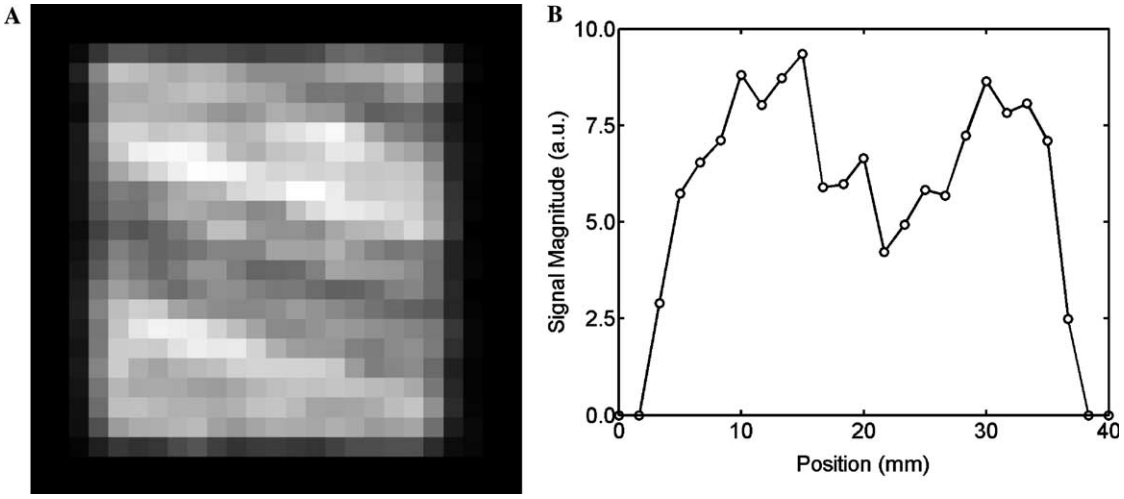

Fig. 3. (A) The 2D magnitude image for a central slice of the Locharbriggs sandstone datasets acquired at an encoding time of 150 μs. (B) Profile (vertical orientation) through the centre of the 2D magnitude image.

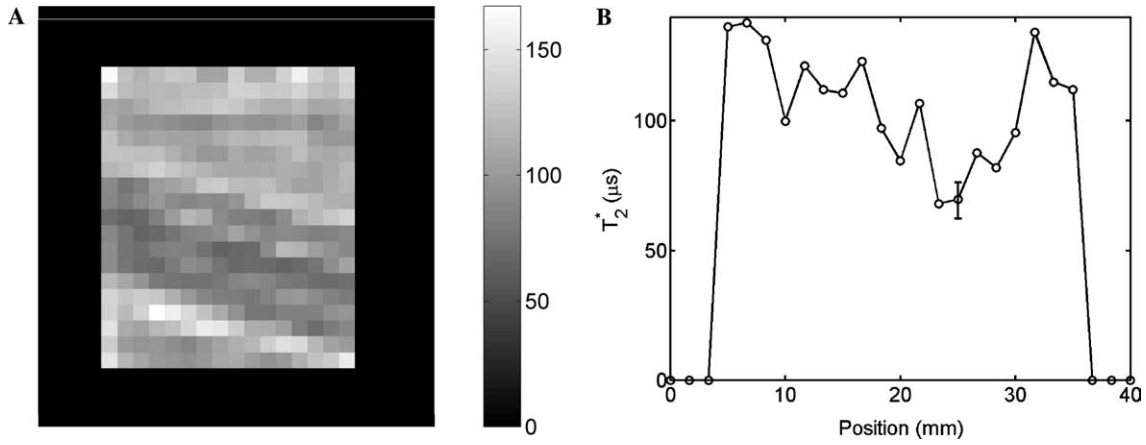

Fig. 5. (A) The 2D T_2^* map corresponding to the same slice of the Locharbriggs sandstone in Fig. 3A. The scale bar is calibrated in units of microseconds. (B) The corresponding vertical 1D T_2^* profile. Only one representative error bar is shown. The line is drawn for guidance only.

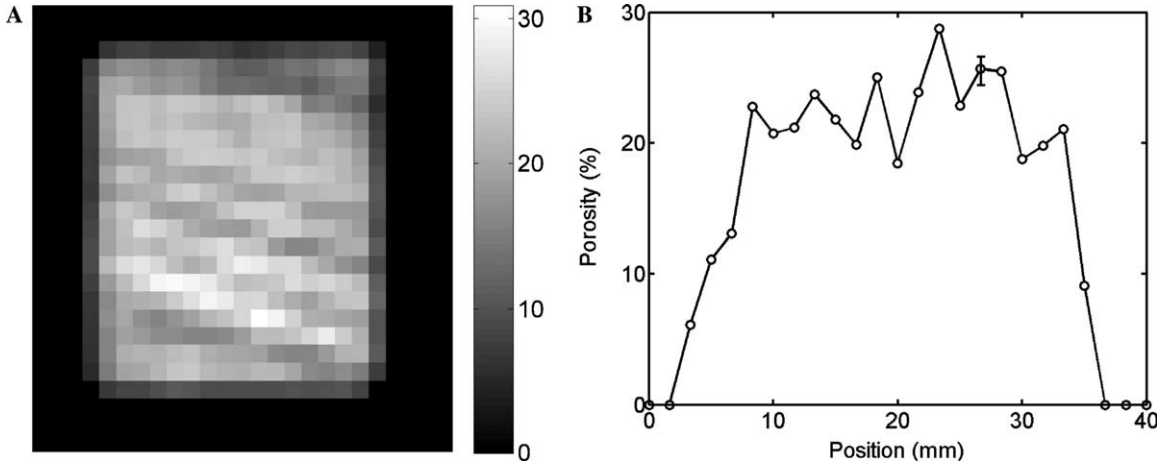

Fig. 6. (A) The resulting 2D porosity map for the same slice of the Locharbriggs sandstone in Fig. 3A. The scale bar is calibrated in units of percent. (B) The vertical 1D porosity profile corresponding to Fig. 5B. The porosity uncertainty is derived from the fit to Eq. (1) and only one representative error bar is shown. The line is drawn for guidance only.

the T_2 decay curves to a biexponential decay model, the T_2 decay is truly a distribution of exponentials.

The centric scan SPRITE method allows reliable measurements of the porosity even for samples characterized by a bedding plane structure. Fig. 3A shows a 2D slice from a 3D image dataset for the Locharbriggs sandstone and Fig. 3B shows a vertical profile though the centre of the magnitude image. Fig. 4 presents the principle of the method in determining porosity: the magnitude of the images was fit on a pixel-by-pixel basis using a monoexponential decay function and the derived porosity image was obtained, after calibration, from the extrapolation of the decay curves to zero encoding time. The fitting, which naturally provides a pixel resolved T_2^*, employed the Nelder–Mead simplex method [18] for χ^2 minimization.

Fig. 5A illustrates the T_2^* map for the same core, obtained by fitting the 16 images acquired with encoding time values between 50 and 600 μs. Fig. 5B shows a vertical T_2^* profile though the centre of the T_2^* map. Extrapolation of the T_2^* mapping data to zero encoding time, Eq. (1), permits the spin density to be extracted and scaled according to the zero-time spin density of the reference phantom. The dark quasi-diagonal region in Fig. 3A reveals a low MRI signal. Although low intensity in the image, this region is in fact high porosity (see Fig. 6A) and the image intensity is low due to a reduced T_2^* value (see Fig. 5A).

Knowing the reference porosity, the ''porosity map'' for each of the studied sandstone cores was generated. Fig. 6A shows the porosity map of the 2D slice chosen, while Fig. 6B displays the vertical porosity profile though the centre of the porosity map for the Locharbriggs sandstone core.

For a direct comparison with the gravimetric-derived porosity, for each sandstone core studied, the mean value and the standard deviation of the MRI-derived porosity of 2D slices using the 2D porosity maps have been calculated (see Fig. 7 and Table 1).

The MRI derived porosity for the Spynie sample agrees with the bulk gravimetric measurement better then the other three, more heterogeneous, samples. It may be that

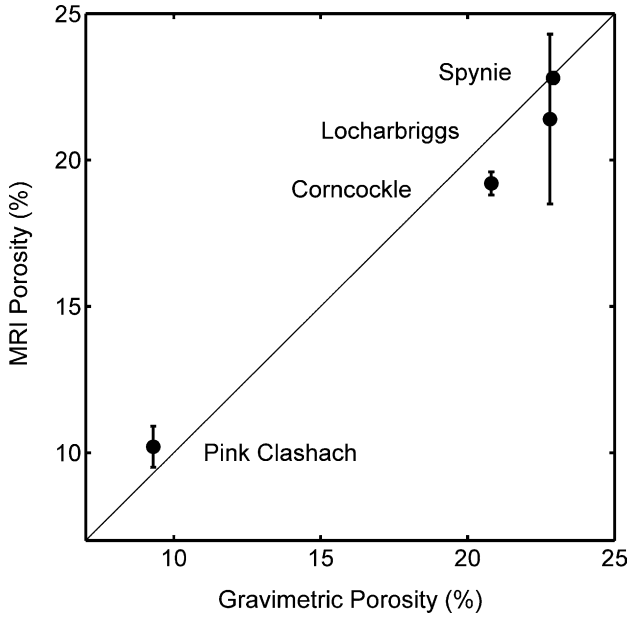

Fig. 7. Average porosity derived through proposed MRI method vs. porosity obtained using the gravimetric method. For Spynie, a relatively homogeneous sandstone (Fig. 2), the conventional and MRI porosity values are identical, within experimental error. For heterogeneous samples, the agreement with bulk measurement is better then 2% absolute porosity. The spread in porosity within the sample, indicated by the error bars, suggests that bulk porosity is a poor indicator of local porosity. The uncertainty in the gravimetric porosity is smaller than the data symbol size.

Table 1
Comparison of MRI- and gravimetric-derived porosities

Type of material	Porosity (%) (gravimetric)[a]	Porosity (%) (MRI)[b]
Locharbriggs	22.8 ± 0.1	21.4 ± 2.9
Spynie	22.9 ± 0.1	22.8 ± 0.2
Corncockle	20.8 ± 0.1	19.2 ± 0.4
Pink Clashach	9.3 ± 0.1	10.2 ± 0.7
Reference phantom	25.0 ± 0.1	—

[a] Data are presented as means ± standard deviation.
[b] Local heterogeneities, as shown in Fig. 6B, have porosities which vary from 11.7 to 29.4. The mean porosity and associated uncertainty (standard deviation) are derived from 2D porosity maps corresponding to individual representative 2D MRI slices from a 3D data set.

the high porosity and relatively large T_2^* of Spynie permit better ρ_0 fitting. However, the agreement in all four samples is remarkably good, less than 2% absolute porosity difference in all cases. The error bars (Fig. 7) and the standard deviations (Table 1) describe the range of porosities found in a representative slice, being measures of the dispersion of local porosity values around the mean.

4. Conclusions

A new noninvasive method for measuring global and local porosity by means of MRI has been presented and validated. The SPRITE imaging technique has proven to be a very robust and flexible method for the study of a wide range of systems with short signal lifetimes. The technique was applied for porosity measurements of four fluid saturated sandstones. Proton density and T_2^* values were extracted from T_2^* mapping. The MRI derived porosity for all samples are in agreement within 2% with the bulk gravimetric measurement. It is anticipated that these methods will be quite generally applicable in determining porosity of fluid saturated porous media. However, we consider that it is important to systematically compare SPRITE to other MRI materials imaging methods where there is a reason to expect competitive results, most naturally with FID-based projection reconstruction.

5. Experimental

Sandstone cores (cylindrical, diameter 3.75 cm, lengths 4–6 cm) were saturated with distilled water under vacuum, in addition to prolonged immersion in boiling water [1].

Conventional porosity measurements were realized using a gravimetric technique (the difference between the mass of the fully water saturated core and of the dry core, divided by the volume). We minimized the effects of natural drying during measurement by wrapping the cores with Teflon tape.

The local image intensity was calibrated with an external reference constituted from H_2O/D_2O simulating 25% porosity. The reference was doped with 20 mM $MnSO_4$ to match the sandstone core relaxation times. After doping, the reference T_1 was 5.2 ms, T_2 was 360 μs and T_2^* was 251 μs.

All NMR and MRI measurements were performed using a MARAN-DRX 7T MRI system (Resonance Instruments, Witney, UK) operating at a proton frequency of 299.65 MHz, with a 7.0 T, 160 mm bore actively screened magnet system provided by Magnex Scientific (Oxford, UK). Magnetic field gradients of up to 40 G/cm were provided by a self-shielded Magnex gradient set, SGRAD 156/100/S. A 6.2-cm home built birdcage RF resonator was used for both radiofrequency transmission and reception. The π/2 pulse length for this probe was 78 μs. The 400 W NMRplus RF power amplifier (model 8T400) was provided by Communication Power (Brentwood, NY).

The bulk T_2^* values were obtained by fitting the free induction decays. The cores were imaged using the 3D Conical SPRITE sequence. The primary image data was 64^3 with an isotropic field of view of $9 \times 9 \times 9$ cm^3 and, consequently, the nominal pixel resolution was 1.4 mm/pixel (Fig. 2); all displayed images were cropped to remove the reference. Fig. 2 and the inset of Fig. 4 show 2D slices, which have been smoothed by zero-filling to 256^3, but not filtered. Figs. 3, 5, and 6 show the raw images and derived image data sets with no image processing or smoothing.

The measurement time was 8 min for 2 scans ($x\bar{x}$ phase cycle), with encoding times varying between 50 and 1100 μs, the repetition time (TR) was 4.5 ms, and the highest magnetic field gradient was 20 G/m. The flip angle was

4°, which is the optimal flip angle for a given TR/T_1 in order to maximize SNR with a minimum blurring, based on point spread function simulations for Conical SPRITE [19].

All data processing was performed offline using various routines written with the Interactive Data Language (Research Systems, Boulder, CO).

Acknowledgments

This work was supported by equipment and operating grants awarded to B.J.B. by NSERC of Canada. B.J.B. also thanks the Canada Chairs program for a Research Chair in MRI of Materials (2002–2007). The UNB MRI Centre is supported by an NSERC Major Facilities Access grant. T.A. and B.J.B. are grateful to the Canada Foundation for Innovation and to the Atlantic Innovation Fund (AIF). F.M. thanks AIF for financial support and is grateful to Dr. Bryce MacMillan for stimulating discussions. CH and AH thank the UK EPSRC and the Royal Society for support and Dr. Ewan Hyslop, British Geological Survey, Edinburgh for petrological data.

References

[1] C. Hall, W.D. Hoff, Water Transport in Brick, Stone and Concrete, Spon Press, London, 2002.
[2] R. Kulkarni, A. Ted Watson, Robust technique for quantification of NMR imaging data, AIChE J. 43 (1997) 2137–2140.
[3] A. Ted Watson, C.T. Philip Chang, Characterizing porous media with NMR methods, Prog. NMR Spectrosc. 31 (1997) 343–386.
[4] W.P. Rothwell, H.J. Vinegar, Petrophysical applications of NMR imaging, Appl. Opt. 24 (1985) 3969–3972.
[5] S. Chen, K.-H. Kim, F. Qin, A.T. Watson, Quantitative NMR imaging of multiphase flow in porous media, Magn. Reson. Imaging 10 (1992) 815–826.
[6] M.R. Merrill, Porosity measurements in natural porous rocks using magnetic-resonance-imaging, Appl. Magn. Reson. 5 (1993) 307–321.
[7] G.C. Borgia, V. Bortolotti, P. Dattilo, P. Fantazzini, G. Maddinelli, Quantitative determination of porosity: a local assessment by NMR imaging techniques, Magn. Reson. Imaging 14 (1996) 919–921.
[8] M.D. Hürlimann, K.G. Helmer, L.L. Latour, C.H. Sotak, Restricted diffusion in sedimentary rocks. Determination of surface-area-to-volume ratio and surface relaxivity, J. Magn. Reson. A 111 (1994) 169–178.
[9] Q. Chen, A.E. Marble, B.G. Colpitts, B.J. Balcom, The internal magnetic field distribution, and single exponential magnetic resonance free induction decay, in rocks, J. Magn. Reson. 175 (2005) 300–308.
[10] D.E. Woessner, Nuclear magnetic resonance spin–echo self-diffusion measurements on fluids undergoing restricted diffusion, J. Phys. Chem. 67 (1963) 1365–1367.
[11] H. Van As, D. van Dusschoten, NMR methods for imaging of transport processes in micro-porous systems, Geoderma 80 (1997) 389–403.
[12] M. Peyron, G.K. Pierens, A.J. Lucas, L.D. Hall, G.F. Potter, R.C. Steward, D.W. Phelps, Strategies for overcoming linewidth limitations in quantitative petrophysical NMR measurements, Magn. Reson. Imaging 12 (1994) 295–298.
[13] R.L. Kleinberg, W.E. Kenyon, P.P. Mitra, Mechanism of NMR relaxation of fluids in rock, J. Magn. Reson. A 108 (1994) 206–214.
[14] B.J. Balcom, R.P. MacGregor, S.D. Beyea, D.P. Green, R.L. Armstrong, T.W. Bremner, Single point ramped imaging with T_1 enhancement (SPRITE), J. Magn. Res. A 123 (1996) 131–134.
[15] S.D. Beyea, B.J. Balcom, P.J. Prado, A.R. Cross, C.B. Kennedy, R.L. Armstrong, T.W. Bremner, Relaxation time mapping of short T_2^* nuclei with single-point imaging (SPI) methods, J. Magn. Reson. 135 (1998) 156–164.
[16] M. Halse, D.J. Goodyear, B. MacMillan, P. Szomolanyi, D. Matheson, B.J. Balcom, Centric scan SPRITE magnetic resonance imaging, J. Magn. Reson. 165 (2003) 219–229.
[17] I.V. Mastikhin, H. Mullally, B. MacMillan, B.J. Balcom, Water content profiles with a 1D centric SPRITE acquisition, J. Magn. Reson. 156 (2002) 122–130.
[18] J.A. Nelder, R. Mead, A simplex method for function minimization, Comput. J. 7 (1965) 308–313.
[19] M. Halse, J. Rioux, S. Romanzetti, J. Kaffanke, B. MacMillan, I. Mastikhin, N.J. Shah, E. Aubanel, B.J. Balcom, Centric scan SPRITE magnetic resonance imaging: optimization of SNR, resolution and relaxation time mapping, J. Magn. Reson. 169 (2004) 102–117.